HHS Public Access

Author manuscript

Acta Biomater. Author manuscript; available in PMC 2017 March 01.

Published in final edited form as:

Acta Biomater. 2016 March 1; 32: 198–209. doi:10.1016/j.actbio.2015.12.032.

Cooperative Effects of Fibronectin Matrix Assembly and Initial Cell-Substrate Adhesion Strength in Cellular Self-Assembly

James R. Brennan[a] and **Denise C. Hocking**[a,b,*]

[a]Department of Biomedical Engineering, University of Rochester, Rochester, New York, USA

[b]Department of Pharmacology and Physiology, University of Rochester School of Medicine and Dentistry, Rochester, New York, USA

Abstract

The cell-dependent polymerization of intercellular fibronectin fibrils can stimulate cells to self-assemble into multicellular structures. The local physical cues that support fibronectin-mediated cellular self-assembly are largely unknown. Here, fibronectin matrix analogs were used as synthetic adhesive substrates to model cell-matrix fibronectin fibrils having different integrin-binding specificity, affinity, and/or density. We utilized this model to quantitatively assess the relationship between adhesive forces derived from cell-substrate interactions and the ability of fibronectin fibril assembly to induce cellular self-assembly. Results indicate that the strength of initial, rather than mature, cell-substrate attachments correlates with the ability of substrates to support fibronectin-mediated cellular self-assembly. The cellular response to soluble fibronectin was bimodal and independent of the integrin-binding specificity of the substrate; increasing soluble fibronectin levels above a critical threshold increased aggregate cohesion on permissive substrates. Once aggregates formed, continuous fibronectin polymerization was necessary to maintain cohesion. During self-assembly, soluble fibronectin decreased cell-substrate adhesion strength and induced aggregate cohesion via a Rho-dependent mechanism, suggesting that the balance of contractile forces derived from fibronectin fibrils within cell-cell versus cell-substrate adhesions controls self-assembly and aggregate cohesion. Thus, initial cell-substrate attachment strength may provide a quantitative basis with which to build predictive models of fibronectin-mediated microtissue fabrication on a variety of substrates.

Keywords

fibronectin; extracellular matrix; self-assembly; cell adhesion; biomimetic material

[*]**Corresponding author:** Denise C. Hocking, Ph.D., Box 711, 601 Elmwood Ave., University of Rochester, Rochester, NY 14642, USA. Tel.: +1 (585) 273-1770; FAX: +1 (585) 273-2652; denise_hocking@urmc.rochester.edu.

Disclosures

The authors have no conflicts of interest related to the contents of this manuscript.

1. Introduction

Modular tissue engineering is emerging as a “bottom-up” approach for the de novo fabrication of tissues and organs. In principle, the structural and functional features of complex tissues may be spatially recreated through the directed assembly of smaller, tissue-like building blocks [1]. Fabricating biomimetic units for modular assembly requires developing methods to reproducibly recreate the microstructural features of native tissue. Extracellular matrices (ECMs) are complex networks of proteins and polysaccharides that normally provide the structural and functional framework for cells to organize into three-dimensional (3D) tissue [2]. During embryonic development, cells spontaneously organize into multicellular 3D structures in the absence of applied external forces by a process termed cellular self-assembly [3]. Inducing cells to self-assemble in vitro recapitulates many aspects of native tissue formation by allowing cells to organize into 3D structures using the ECM as a natural scaffold [4]. As such, engineering approaches that utilize cellular self-assembly to promote the spontaneous organization of cells and ECM proteins into functional 3D microtissue units may provide a biologically inspired approach to modular tissue fabrication.

A complex, integrated balance of cell-cell and cell-matrix adhesive interactions generates the mechanical forces and chemical signals necessary to control cell activity and tissue morphology during cellular self-assembly [5-8]. Fibronectin is a principal component of interstitial ECMs and plays a fundamental role in cell adhesion and tissue formation during embryonic development [9]. ECM fibronectin fibrils can localize to either cell-cell [5, 10-12] or cell-matrix [13] adhesions, where they stimulate Rho-mediated cell contractility [14, 15]. Fibronectin fibrils associated with intercellular adhesions support cellular self-assembly by promoting the cohesion of cells into tightly packed 3D clusters [5, 11, 16]. Conversely, fibronectin fibrils that localize basally to cell-matrix adhesions are associated with the disassembly of cadherin-mediated cell-cell contacts [17], enhanced cell migration [18], and tumor cell metastasis [19], indicating a paradoxical role for fibronectin fibrils in cellular dyscohesion. As such, the global balance of forces and signals derived from fibronectin fibrils within either cell-cell or cell-matrix adhesions may be a central determinant of cellular self-assembly, tissue cohesion, and cell aggregate morphology.

The insoluble, fibrillar form of fibronectin is the biologically active conformation of the molecule [20]. The polymerization of inactive, soluble fibronectin protomers into biologically active ECM fibrils occurs via a tightly controlled, cell-dependent process [20]. The bioactivity of ECM fibronectin has been localized, in part, to a matricryptic, heparin-binding site located within the first type III repeat of fibronectin (FNIII1) [21-23]. This bioactive site is inaccessible in soluble fibronectin, but becomes exposed upon polymerization into ECM fibrils [24]. Once assembled, highly elastic ECM fibronectin fibrils can be further remodeled in response to cell and tissue-derived forces [23, 25, 26]. Compressive, tensile and/or shear stresses exerted on polymerized fibronectin fibrils may subsequently alter the spacing and/or availability of cell and protein binding sites within fibronectin fibrils [27], giving rise to a dynamic range of structurally and functionally distinct forms of ECM fibronectin. How different structural or conformational forms of fibrillar fibronectin influence cell and tissue function is only beginning to be understood. Recent studies provide evidence that relaxed fibronectin fibrils are associated with reduced

α5β1 integrin activation [28], decreased cell proliferation [28], and increased cell cohesion [29]. In contrast, stretched/unfolded fibronectin fibrils are associated with enhanced cell proliferation [28] and migration [30], decreased adhesion [31], and enhanced growth factor secretion [31]. Further, manually stretched fibronectin fibers support increased osteogenic differentiation of mesenchymal stem cells [32].

To begin to understand how the balance of adhesive forces derived from conformationally-labile fibronectin fibrils impacts cellular self-assembly, we developed a series of recombinant fibronectin fragments that mimic different conformational states of ECM fibronectin. These fibronectin fragments were produced by directly coupling the open, bioactive heparin-binding fragment of FNIII1 (FNIII1H) to varying portions of the central, integrin-binding domain of fibronectin [33]. In the present study, three different fibronectin matrix analogs were used as synthetic adhesive substrates to model cell-matrix fibronectin fibrils having different integrin-binding specificities and affinities. We utilized this model to investigate how adhesive forces derived from cell-ECM fibronectin adhesions influence the capacity of newly assembled fibronectin fibrils to induce cellular self-assembly. In turn, the impact of varying fibronectin fibril assembly parameters on cellular self-assembly and aggregate cohesion were determined.

2. Materials and Methods

2.1. Recombinant proteins, reagents, and cells

Glutathione S-transferase (GST) and the GST-tagged fusion proteins, FNIII8-10, FNIII1H, 8-10, and FNIII1H,8^{RGD} were produced in *Escherichia coli* and purified using glutathione-Sepharose (GE Healthcare, Piscataway, NJ) affinity chromatography, as described previously [33]. His-tagged functional upstream domain (FUD) and the control peptide, del29 [34] were produced in *Escherichia coli* and purified using Nickel-Sepharose (GE Healthcare). Recombinant fibronectin proteins were produced using human fibronectin cDNA, as described previously [14]. The sequence homology for the same fibronectin type III repeat across multiple species is between ~80-90%. Mouse and human cell attachment domains (i.e., FNIII7-10) show 85% homology [35]; the mouse and human sequences for FNIII1H show 88% homology. No species-dependent differences have been observed when testing recombinant fibronectin proteins with mouse- or human-derived cells [17, 18, 36]. Similarly, ‘human’ recombinant fibronectin proteins have similar functional effects when tested in vivo in both mice and hamsters [23, 37]. Of note, cells obtained from various species (including mouse and human) polymerize fibronectin into insoluble fibronectin fibrils via similar cell-dependent mechanisms [20].

FNIII1H^{RGD} was engineered by inserting the integrin-binding RGD loop between the F and G β strands of FNIII1H, analogous to its native location in FNIII10. FNIII1H is a carboxyl-terminal fragment of the first type III repeat of fibronectin and is comprised of amino acids I^{597} – T^{673} (bases 1802-2032). The RGD chimera, FNIII1H^{RGD} was produced using the following mutant sense primer: 5’-G**GTATAC**GAGGGCCAGCTCATATCGATTCAGGGCCGTGGAGACTCGCCGGCAAGCCAAGAAGTGACTCGCTTTGAC-3’. Bases 1976 to 1987 (Q^{655} to H^{658}) of FNIII1H were replaced with the underlined bases, which encode for amino acids G^{1491}RGDSPAS

from FNIII10, leading to a net addition of 4 amino acids to FNIII1. The FNIII10 insert contains an engineered NgoMIV site as a marker. The BstZ17I site is shown in bold. The antisense primer for GST/III1H^{RGD} (5'-CCC**GAATTC**CTATGTGCTGGTGCTGGTGGTG;-3') contains a EcoRI site, shown in bold. The PCR product of this reaction was ligated into pGEX2T/III1H after removal of the corresponding BstZ17I and EcoRI fragment and cloned into DH5 α bacteria. DNA was sequenced to confirm the presence of the mutation.

Fibronectin was purified from outdated human plasma (American Red Cross, Rochester, NY) using gelatin-Sepharose (GE Healthcare) affinity chromatography [38]. Type I collagen was extracted from rat tail tendons, as described [11]. Anti-GST monoclonal antibody (clone DG122-2A7) was from Millipore; α_5 (clone 5H10–27), α_v (clone H9.2B8), β_1 (clone Ha2/5), and β_3 (clone 2C9.G2) integrin monoclonal antibodies, IgG and IgM controls were from BD Biosciences; anti-fibronectin polyclonal antibody was from Sigma; horseradish peroxidase-conjugated (HRP) goat anti-mouse antibodies were from Bio-Rad. Alexa Fluor^{488}-conjugated goat anti-rabbit IgG was from Life Technologies.

Mouse embryonic fibronectin-null fibroblasts (FN-null MEFs) were cultured on type I collagen-coated dishes using a 1:1 mixture of Cellgro® (Mediatech) and Aim V (Life Sciences). These media do not contain fibronectin and do not require serum-supplementation [39]. Tissue culture plates were coated with recombinant fibronectin fragments diluted in phosphate-buffered saline (PBS) at the indicated concentrations for 90 min at 37°C. Unbound protein was removed, wells were washed with PBS and then blocked with 1% fatty acid-free bovine serum albumin (BSA) for 1 h at 37°C prior to seeding cells. Protein binding was assessed by enzyme-linked immunosorbant assays (ELISA), using the anti-GST antibody, as described [33]. In the absence of serum supplementation, FN-null MEFs do not adhere to non-coated or BSA-coated surfaces [39].

2.2. Cell adhesion assays

Static cell adhesion assays were performed by seeding FN-null MEFs (1.6×10^5 cells/cm^2) onto tissue culture plates (96-well) pre-coated with recombinant fibronectin fragments at various concentrations. Cells were incubated for 4 h at 37°C, then washed and fixed with 1% paraformaldehyde. Cell number was quantified using crystal violet, as described previously [33].

Initial cell-substrate binding strength was measured using centrifugation adhesion assays [40, 41]. FN-null MEFs (1.6×10^5 cells/cm^2) were seeded onto ice-cold tissue culture plates pre-coated with recombinant fibronectin fragments at various concentrations. Cells were immediately centrifuged into contact with the adhesive substrate for 3 min at 700 rpm (99 *g*) at 4° C. Plates were then inverted and centrifuged for 5 min at 1500 rpm (452 *g*) at 4° C. Cell-substrate binding strength was also quantified 24 h post-seeding in the absence and presence of plasma fibronectin. FN-null MEFs (4×10^4 cells/cm^2) were seeded onto tissue culture plates pre-coated with fibronectin fragments at various concentrations. Plasma fibronectin (50 nM) or an equal volume of the vehicle control, PBS, was added to cells at 4 h post-seeding and cells were incubated an additional 20 h at 37°C. Plates were then inverted and centrifuged for 5 min at 1500 rpm (452 *g*) at 25°C. After centrifugation, cells

were washed, fixed, and stained with crystal violet to quantify the number of adherent cells. Adhesion profiles were fit to a sigmoidal curve and the substrate coating concentrations that supported half-maximal adhesion (C^{c50}) were determined using GraphPad Prism. The parameter C^{c50} represents an inverse adhesive affinity for the substrate and was used as a measure of adhesion strength to compare different substrates [42].

2.3. Cellular self-assembly assays

FN-null MEFs (2×10^4 cells/cm^2) were seeded onto 35 mm tissue culture plates pre-coated with the recombinant fibronectin fragments at various concentrations. Cells were allowed to adhere for 4 or 24 h to allow cell adhesion strength to attain steady-state levels [43] before plasma fibronectin treatment. Aliquots of plasma fibronectin (6.25 - 100 nM) or an equal volume of the vehicle control, PBS, were added and cells were incubated at 37°C and 8% CO_2 for various times. To determine the role of Rho, the p160-Rho-associated coiled kinase (ROCK) inhibitor, Y-27632 (10 μm, Tocris) [44], or an equal volume of the vehicle, PBS was added to cells immediately after seeding. To determine the role of fibronectin matrix assembly, FUD or del29 peptides (250 nM) were added to fibronectin-treated wells 72 h post-seeding. Phase contrast microscopy images were obtained using a MicroPublisher digital camera (QImaging) on an Olympus IX70 microscrope at various time points post-seeding. Aggregate diameter was quantified using ImageJ (NIH) by measuring the major and minor diameter of each spheroid and determining the average value. For each independent experiment, at least 30 spheroids were measured per condition.

2.4. Immunofluorescence microscopy

FN-null MEFs (2×10^4 cells/cm^2) were seeded onto protein-coated plates. Plasma fibronectin (25 nM) was added 4 h post-seeding. At various times, cells were then fixed with 4% paraformaldehyde, and processed for immunofluorescence microscopy [21]. Fibronectin within flat cellular networks was visualized using a BX60 Olympus microscope and images were obtained using an EXi Blue Fluorescence Microscopy Camera (QImaging). Fibronectin within 3D aggregates was visualized using multi-photon microscopy, using an Olympus Fluoview 1000 AOM-MPM microscope (Olympus), as described previously [11].

2.5. Statistical analyses

Data are presented as mean ± standard error of the mean (SEM). Experiments were performed in triplicate a minimum of 3 times. Statistical comparisons were performed using one-way analysis of variance (ANOVA) followed by the Bonferroni post-test or Student's t-test for unpaired samples, as appropriate, with GraphPad Prism Version 4 software. Results were considered statistically significant when $p < 0.05$.

3. Results

3.1. Substrate-dependent effects on cellular self-assembly and aggregate size

Three recombinant fibronectin matrix mimetics (FNIII1H,8-10, FNIII1H,8^{RGD}, and FNIII1H^{RGD}; Fig. 1A) were used as defined adhesive substrates to model ECM fibronectin fibrils having different integrin-binding specificities and affinities. Common to all 3 fibronectin constructs is the open, bioactive heparin-binding fragment of FNIII1 (FNIII1H)

that mediates effects of ECM fibronectin fibrils on cell and tissue function [22]. The integrin-binding capacity of the different fibronectin matrix mimetics was varied by selectively incorporating different portions of the central, integrin-binding domain of fibronectin (spanning modules FNIII8, FNIII9, and FNIII10 [45]) into the final construct [33]. Thus, only the basic αvβ3 integrin-binding RGD loop [46] is available to mediate cell adhesion in the smallest matrix mimetic, FNIII1H^{RGD} (Fig. 1B). A larger construct, FNIII1H,8^{RGD}, was produced by inserting the RGD loop into the analogous site in FNIII8. This construct provides a more complex integrin-binding surface [47, 48], yet still mediates cell adhesion via αvβ3-integrins [36]. The largest matrix mimetic, FNIII1H,8-10, contains all 3 integrin-binding modules (FNIII8, FNIII9, and FNIII10) and mediates cell adhesion selectively via α5β1 integrins [36]. Previous studies provide evidence that fibronectin fibril extension favors cell adhesion via αvβ3 over α5β1 integrins [31, 49], likely by increasing the interdomain distance between the FNIII9 and FNIII10 modules [50, 51]. Thus, FNIII1H^{RGD} serves as a relatively simple, 2D model of extended-unfolded fibronectin fibrils with limited integrin binding potential, while FNIII1H,8-10 serves as a model of extended-compact fibrils with a fully exposed integrin-binding face.

All 3 fibronectin matrix mimetics bound to tissue culture wells with similar efficiency over a range of coating concentrations (Fig. 1C). Similarly, in static adhesion assays, all 3 matrix mimetic substrates supported cell adhesion to a similar extent, as no significant differences were observed in the number of cells adherent to wells pre-coated with the various proteins at concentrations ≥ 25 nM (Fig. 1D). The use of recombinant fibronectin substrates in combination with FN-null MEFs allows for precise control over the adhesive substrate, the amount of soluble fibronectin available to cells, as well as the matrix assembly process. This combined approach provides a well-defined background with which to investigate the relative contributions of cell adhesion parameters on fibronectin-mediated cellular self-assembly.

The cell-mediated process of polymerizing soluble fibronectin into insoluble fibrils can trigger the coalescence of cells into multicellular aggregates when cells are either non-adherent or adherent to highly compliant surfaces [5, 11]. In the present study, cells were seeded onto rigid tissue culture wells pre-coated with fibronectin matrix mimetics in order to eliminate the contribution of substrate compliance on cellular self-assembly. A range of substrate coating concentrations (12.5 nM – 800 nM) was tested to determine whether substrate ligand density contributes to self-assembly. No obvious differences in either cell attachment or spreading were observed microscopically at the time of fibronectin addition for the range of coating concentrations tested (not shown). In the absence of soluble full-length fibronectin, FN-null MEFs adherent to FNIII1H^{RGD}, FNIII1H,8^{RGD}, or FNIII-1H, 8-10 remained as individual cells for at least 72 h post-seeding (not shown). In contrast, addition of soluble, full-length fibronectin (25 nM; 12.5 μg/ml) to cells 4 h after seeding triggered cellular self-assembly by a mechanism that was dependent on substrate coating density (Fig. 2). Both αvβ3 (FNIII1H^{RGD}, FNIII1H,8^{RGD}) and α5β1 (FNIII-1H,8-10) integrin-binding substrates supported cellular self-assembly (Fig. 2). However, the range of coating densities that supported self-assembly differed among the substrates. In response to fibronectin, cellular self-assembly was observed in wells coated with ≤ 400 nM FNIII1H^{RGD}, ≤ 100 nM FNIII1H,8^{RGD}, and ≤ 25 nM FNIII1H,8-10 (Fig. 2). For all

substrates, coating densities above these values led to the formation of flat, confluent monolayers (Fig. 2). Thus, an inverse relationship was observed between the number of integrin-binding motifs present in the adhesive ligand and the ligand densities that supported cellular self-assembly. These results suggest that on rigid (non-compliant) surfaces, a transition density exists for each adhesive substrate, below which soluble fibronectin can trigger cellular self-assembly, but above which, cells form 2D monolayers.

Aggregate diameter varied directly with both substrate ligand density and number of the integrin-binding motifs (Fig. 3). A dose-dependent increase in aggregate diameter was observed for coating concentrations of FNIII1H^{RGD} that supported fibronectin-induced cellular self-assembly (Fig. 3A; 12.5 – 400 nM). Similarly, average aggregate diameter increased with increasing coating concentrations of FNIII1H,8^{RGD} (12.5 - 100 nM) and FNIII1H,8-10 (12.5 and 25 nM) (Fig. 3B). Cellular aggregates that formed on wells coated with FNIII1H,8-10 were significantly larger than those formed at comparable coating concentrations of FNIII1H^{RGD} and FNIII1H,8^{RGD} (Fig. 3B). Similarly, at coating concentrations of 50 nM and 100 nM, cellular aggregates formed on FNIII1H,8^{RGD} were significantly larger than those formed on FNIII1H^{RGD} (Fig. 3B). For all substrates tested, aggregate diameter peaked at ~ 100 μm.

3.2. Initial cell-binding strength and cellular self-assembly

Thus far, data indicate that effects of substrate density on cellular self-assembly correlate with the number of integrin-binding motifs within the adhesive ligand. Hence, we sought to identify a quantitative parameter characteristic of the adhesive ligand that could be indicative of self-assembly behavior. A centrifugal cell adhesion assay was performed to determine the relative initial cell-binding strengths of the fibronectin matrix mimetics. Cells were centrifuged into contact with the adhesive substrate briefly, and then immediately subjected to a de-adhesion force of ~300 pN, shown previously to be sufficient to dislodge 50% of fibrosarcoma cells from fibronectin-coated wells [41]. By holding the detachment force constant while varying substrate and substrate coating concentrations, the effects of substrate chemistry on cell-substrate attachment can be assessed [41]. At 4°C, cell attachment occurred at lower coating concentrations of FNIII1H,8-10 than FNIII1H,8^{RGD} or FNIII1H^{RGD}, and at lower coating concentrations of FNIII1H,8^{RGD} than FNIII1H^{RGD} (Fig. 4). Thus, cell attachment became more efficient as the number of integrin-binding motifs within the adhesive ligand increased. A single quantitative value (C^{c50}) representing the inverse adhesive affinity was determined by calculating the coating concentration required for half-maximal adhesion (Table 1). The ‘initial’ C^{c50} allows for comparisons of the initial cell attachment strength of substrates prior to cell spreading and cytoskeletal coupling [52]. Notably, the initial C^{c50} value of each substrate fell between the coating concentrations at which fibronectin-treated cells transitioned from self-assembled 3D aggregates to flat sheets (shown in Fig. 2). Thus, initial adhesion strength may serve to predict the transition density for cellular self-assembly.

3.3. Fibronectin-dependent effects on cellular self-assembly and aggregate cohesion

We next evaluated how cellular self-assembly and substrate transition densities were affected as several different fibronectin fibril assembly parameters were varied. First, to

determine whether the amount of soluble fibronectin available to cells alters the substrate transition density for fibronectin-mediated cellular self-assembly, FN-null MEFs were seeded on plates pre-coated with the fibronectin matrix mimetics at concentrations above and below the initial C^{c50}. Cells were allowed to adhere and spread for 4 h and then treated with increasing concentrations of soluble fibronectin (6.25 nM - 100 nM). For all 3 adhesive ligands, substrate coating concentrations below the C^{c50} supported cellular self-assembly at fibronectin concentrations > 12.5 nM (Fig. 5). In contrast, cells adherent to substrates coated above the C^{c50} formed flat monolayers over the range of fibronectin concentrations tested (Fig. 5). These data reveal a bimodal response to fibronectin wherein a minimum level of soluble fibronectin was required to trigger cellular self-assembly. On surfaces permissive for self-assembly, higher fibronectin concentrations resulted in more cohesive aggregates, with a reduction in cell protrusions onto the substrate surface (Fig. 5).

We next asked whether initiating fibronectin matrix assembly at later stages of cell adhesion and spreading affects the ability of fibronectin to induce cellular self-assembly. Cells were allowed to adhere on wells coated with various concentrations of $FNIII1H,8^{RGD}$ for either 4 h or 24 h [22] prior to fibronectin addition. Addition of soluble fibronectin to cells 24 h after seeding did not alter the ability of fibronectin to induce self-assembly (Fig. 6; 24h, +FN). Moreover, substrate coating concentrations that supported fibronectin-mediated self-assembly were identical for both treatment protocols (Fig. 6; 25 - 100 nM), indicating that the substrate transition density for cellular self-assembly did not shift upon formation of mature cell adhesions.

Finally, to determine whether continuous fibronectin matrix assembly is necessary to maintain aggregate cohesion, FN-null MEFs were seeded onto plates pre-coated with $FNIII1H^{RGD}$ and then treated with fibronectin for 3 days to allow for self-assembly. Fibronectin fibril formation over this time period was visualized using confocal immunofluorescence microscopy. As shown in Figure 7, fibronectin fibrils were present at all time points; fibronectin staining was also visible within the central region of the 3D aggregates (Fig. 7C,D). Upon formation of multicellular aggregates (Fig. 8; 72h), fibronectin matrix assembly was blocked by addition of a peptide inhibitor (FUD) and aggregate morphology was monitored for an additional 2 days. FUD peptides bind to soluble fibronectin, inhibiting fibronectin matrix assembly [34], and triggering turnover of previously established fibronectin fibrils [53]. Control wells were treated with the inactive peptide, del29 [34]. Inhibiting fibronectin matrix assembly resulted in the dispersal of cells from aggregates within 1 day of treatment (Fig. 8; +FUD, 96 h and 120 h). In contrast, aggregates remained cohesive in the presence of the inactive control peptide, del29 (Fig. 8; +del29). Taken together, these data indicate that fibronectin levels determine the extent of aggregate cohesivity and that continuous fibronectin matrix assembly is required to maintain aggregate cohesion.

3.4. Effect of fibronectin on cell-substrate binding strength

The balance of contractile forces within cell-cell and cell-matrix adhesions is thought to mediate cellular self-assembly [54]. If so, then fibronectin-mediated contraction within intercellular adhesions during the early stages of self-assembly should be accompanied by a

corresponding decrease in cell-substrate adhesion strength. To quantify effects of fibronectin on cell-substrate binding strength, centrifugal adhesion assays were performed 20 h after fibronectin addition (24 h after initial cell seeding), prior to the formation of 3D structures. Addition of fibronectin to cells caused a rightward shift of cell adhesion curves only at coating concentrations that were permissive for self-assembly, *i.e.*, at concentrations less than the initial C^{c50} (Fig. 9; dotted lines denote initial C^{c50}). In contrast, no significant differences in cell adhesion in response to fibronectin were observed at coating concentrations that were not permissive for self-assembly, *i.e.* concentrations greater than the initial C^{c50} (Fig. 9).

Cell adhesion strength at 24 h was quantified for cells cultured in the absence or presence of fibronectin on each of the fibronectin matrix mimetic substrates; results are shown in Table 1. In the absence of fibronectin, 24 h C^{c50} values of cells adherent to FNIII1H,8^{RGD} and FNIII1H^{RGD} were less than their initial C^{c50} values, demonstrating an increase in adhesion strength over time, as observed previously [43]. Moreover, addition of fibronectin for 20 h to cells adherent to FNIII1H,8^{RGD} and FNIII1H^{RGD} resulted in a significant increase in the 24 h C^{c50}, demonstrating an overall reduction in cell adhesion strength with fibronectin treatment. In contrast, the initial C^{c50} for FNIII1H,8-10-coated substrates was not significantly different from values obtained at 24 h, either in the absence or presence of fibronectin, consistent with the inability of this substrate to support self-assembly behavior at all but the lowest coating concentrations (Fig. 2).

Rho-mediated contraction contributes to the assembly of non-adherent cells into cohesive aggregates [7] and fibronectin fibril assembly has been shown to stimulate Rho-mediated cell contractility [14]. To determine whether Rho activity is necessary for fibronectin-dependent cellular self-assembly, cells were seeded onto wells coated with FNIII1H^{RGD} at 2 different concentrations below the initial C^{c50}. The chemical inhibitor Y-27632 was used to inhibit rho-associated protein kinase (ROCK), a downstream effector of Rho [44]. Addition of Y-27632 inhibited aggregate formation in response to fibronectin (Fig. 10; A-D). The inhibition of self-assembly was not due to an inhibition of fibronectin matrix polymerization, as Y-27632-treated cells assembled intercellular fibronectin fibrils to a similar extent as non-treated cells (Fig. 10; E, F). These data indicate that Rho activity is necessary for fibronectin-dependent cellular self-assembly and suggest that fibronectin fibril-mediated Rho activation within intercellular adhesions leads to cell-substrate detachment and drives self-assembly on adhesive surfaces.

4. Discussion

In this study, we show that fibronectin-mediated cellular self-assembly can be stimulated on rigid, adhesive surfaces under conditions defined by the initial cell attachment strength. An inverse relationship was observed between the number of integrin-binding motifs present within the underlying adhesive substrate and the ligand densities that supported cellular self-assembly. Cellular self-assembly occurred on both $\alpha v\beta 3$ and $\alpha 5\beta 1$ integrin-binding substrates. Thus, the integrin-binding avidity of the adhesive substrate, rather than the integrin-binding specificity, contributes to self-assembly behavior. A transition ligand density, quantified in the present study as the initial C^{c50}, was identified for each adhesive

ligand, below which soluble fibronectin triggered cellular self-assembly into 3D multicellular structures, and above which, cells remained as 2D monolayers. Neither the amount of soluble fibronectin available to cells nor the time at which fibronectin matrix assembly was initiated altered the substrate transition density for self-assembly. Thus, the initial cell-substrate adhesion strength, derived from centrifugal adhesion assays, appears to serve as a simple, quantifiable parameter with which to determine substrate densities that support fibronectin-mediated cellular self-assembly. Aggregate diameter varied directly with both substrate ligand density and number of the integrin-binding motifs, suggesting that tuning initial substrate adhesion strength may serve to produce microtissue units of defined diameter. These microtissue units are easily removed from the initial adhesive substrate by mechanical dissociation and can be reseeded onto new adhesive substrates or into non-adhesive wells. Three-dimensional microtissues are emerging as physiologic, 3D organ models (e.g., “organ-on-a chip”) for basic science research and high-throughput drug screening. Additionally, embedding multiple microtissue units into hydrogel scaffolds to form small tissues is emerging as a potential method for repairing small tissue defects, and may eventually find wide-spread use in whole organ printing [55]. Our results provide key design criteria that can be incorporated into a variety of cell culture platforms to produce microtissue units of defined dimensions. Specifically, we have shown that initial cell-substrate adhesion strength and fibronectin matrix assembly are cooperative parameters that can be modulated to influence both the formation and dimension of microtissue units.

In the present study, the cellular response to soluble fibronectin concentration was bimodal and similar on all substrates tested, with fibronectin concentrations as low as 12.5 nM (6.25 μg/ml) stimulating 3D aggregate formation. Increasing fibronectin concentration above this level resulted in smaller areas of peripheral cell extensions onto the adhesive substrate, confirming that fibronectin concentration plays a role in determining the level of microtissue cohesion [5, 11]. The reported dissociation constant for the initial binding of the amino-terminus of fibronectin to the cell surface ranges from $1.5 – 4 \times 10^{-8}$ M [56]. Thus, the concentration of soluble fibronectin required to initiate cellular self-assembly is in close agreement with that required to initiate fibronectin matrix assembly. Continuous fibronectin fibril assembly was necessary to maintain aggregate cohesion, as inhibiting fibronectin matrix assembly in pre-formed aggregates led to cell dispersal onto the adhesive substrate. For these studies, we utilized mouse embryonic fibroblasts that do not produce fibronectin in order to control the amount of exogenous fibronectin to which the cells are exposed and the timing of the fibronectin polymerization process. Fibronectin-dependent cellular self-assembly is emerging as a common morphological process, as it has been observed in several cell types, including primary fibroblasts [16], a variety of cell lines [5, 54], as well as mixed cell populations [57]. Recent studies have demonstrated a role for fibronectin matrix assembly in mesenchymal stem cell condensation [58], while other studies suggest that disruption of fibronectin-mediated cohesion may play a role in tumor metastasis [59]. As such, understanding how cell-substrate adhesion parameters cooperate with fibronectin matrix assembly to dynamically regulate the level of tissue or tumor cohesion or dyscohesion has implications in a variety of physiological and pathological processes, and may provide new avenues for therapeutic intervention.

Fibronectin fibrils associated with 3D cell aggregates localize to intercellular spaces [29] via an α5β1 integrin-dependent process [5]. Thus, non-cadherin-based cell-cell adhesions can be formed via pericellular fibronectin fibrils that indirectly link adjacent cells together via integrin receptors. However, continuous assembly of fibronectin fibrils is necessary to maintain these atypical cell-cell connections. Fibronectin fibril polymerization is an active process that undergoes successive rounds of fibril assembly, maturation, and turnover [60], while the rate and extent of fibronectin formation can also be rapidly up- or down-regulated [20]. These dynamic properties may provide a mechanism for cells to transition fluidly from 2D to 3D states and visa versa, as shown in Supplemental Figure and Video 1.

Fibronectin-induced cellular self-assembly has been observed previously using either non-adhesive cell culture platforms [5] or compliant collagen gels to mediate cell attachment [11, 16]. Here, we demonstrate that fibronectin-mediated cellular self-assembly can also be induced on rigid adhesive substrates if the substrate coating concentration is adjusted to produce an initial cell-substrate adhesion strength that is approximately half the maximum value. For all substrates tested, cell-substrate adhesion strength increased to similar levels after a 24 h period, consistent with previous studies demonstrating that cell adhesion strength reaches a steady state within 4 hours of seeding [43]. In contrast, the coalescence of cells into fully 3D aggregates was not apparent until ~24-36 h after fibronectin addition (Supplemental Video 1). Importantly, addition of soluble fibronectin to adherent cells reduced cell adhesion strength by 24 h for substrate coating concentrations that were permissive for self-assembly, providing evidence that polymerization of fibronectin fibrils at intercellular spaces reduces cell-substrate adhesion strength prior to the transition to 3D. The ability of the ROCK inhibitor to block fibronectin-induced 3D aggregate formation suggests that Rho-mediated contractility, generated at sites of cell-cell contact by fibronectin fibrils [14], exerts a force sufficient to overcome cell-substrate bonds at nascent adhesions. Once 3D clusters begin to form, cohesive forces between non-adherent cells are shared, while cells that remain adherent to the underlying substrate exert stronger attractive forces upon their nearest neighbors on the adhesive surface. Thus, surface tension generated upon 3D cell cluster formation may provide additional de-adhesive forces that break cell-matrix attachments. On permissive surfaces, spheroid diameter increased with increasing ligand density and increasing initial adhesion strength, providing evidence that spheroid size is determined by the difference between cell-substrate bonds at nascent adhesions and the collective strength of cell-cell cohesive forces.

Results of our study imply that both the local density and conformation of fibronectin fibrils within cell-matrix adhesions impact the location and subsequent function of newly polymerized fibronectin fibrils. Addition of fibronectin to adherent cells decreased cell-substrate binding strength, but only on low-adhesion substrate coating concentrations that permitted self-assembly. These data suggest that when local microenvironmental conditions are conducive to developing nascent adhesions of low binding strength, cells localize fibronectin fibrils preferentially within intercellular junctions, where Rho-mediated contraction strengthens cell-cell contacts and exerts a de-adhesive force on cell-substrate contacts. Conversely, cells subjected to conditions of high nascent adhesion-strength localize fibronectin to cell-substrate adhesions, strengthening cell-matrix contacts and reducing cell-cell contacts [17]. Similar to the process of fibronectin matrix polymerization,

cell-substrate adhesions undergo successive rounds of initiation and maturation, beginning at the leading edge of the cell [61]. Thus, the tight correlation between initial cell attachment strength and cellular self-assembly suggests that as cells begin to organize in 2D, newly formed nascent cell adhesions at the leading edge of the cell are those most likely to be disrupted by contractile forces generated during the polymerization of fibronectin fibrils; the repeated disruption of leading edge contacts can be clearly observed in Supplemental Video 1. Importantly, our studies demonstrate that the polymerization of fibronectin fibrils can initiate cellular self-assembly under a range of adhesion conditions. Moreover, the attachment strength of initial/early adhesions may determine whether fibronectin fibrils and α5β1 integrins localize to cell-cell or cell-matrix adhesions, and function therein, possibly through changes in cell signaling that are associated with the transition to 3D [62].

5. Conclusion

Substrate ligand composition and density play cooperative roles with cell-mediated fibronectin matrix polymerization to control the transition of cells from 2D monolayers into 3D multicellular aggregates. The strength of initial cell-substrate attachment, determined from centrifugal adhesion assays and defined by the initial C^{c50}, correlated with the ability of adhesive substrates to support fibronectin-dependent cellular self-assembly. Three-dimensional microtissues are emerging as physiologic models for basic science research and high-throughput drug screening, and may provide a bottom-up approach for de novo tissue fabrication. Results of the current study provide a quantitative basis with which to build predictive models of microtissue assembly, as well as a simple cell-culture platform to produce uniform biomimetic units for modular tissue engineering.

Supplementary Material

Refer to Web version on PubMed Central for supplementary material.

Acknowledgements

This work was supported in part by grant EB018210 from the National Institutes of Health. JRB received support from the Harold C. Hodge Memorial Fund through the Department of Pharmacology and Physiology. The authors thank Susan Wilke-Mounts for excellent technical assistance.

Abbreviations used

ECM	extracellular matrix
FNIII	fibronectin type III repeat
GST	glutathione-S-transferase
FN	fibronectin

References

[1]. Nichol JW, Khademhosseini A. Modular tissue engineering: engineering biological tissues from the bottom up. Soft Matter. 2009; 5:1312–1319. [PubMed: 20179781]

[2]. Rozario T, DeSimone DW. The extracellular matrix in development and morphogenesis: a dynamic view. Dev Biol. 2009; 341:126–140. [PubMed: 19854168]

[3]. Hall BK, Miyake T. All for one and one for all: condensations and the initiation of skeletal development. BioEssays. 2000; 22:138–147. [PubMed: 10655033]

[4]. Athanasiou KA, Eswaramoorthy R, Hadidi P, Hu JC. Self-organization and the self-assembling process in tissue engineering. Annu Rev Biomed Eng. 2013; 15:115–136. [PubMed: 23701238]

[5]. Robinson EE, Foty RA, Corbett SA. Fibronectin matrix assembly regulates alpha5beta1-mediated cell cohesion. Mol Biol Cell. 2004; 15:973–981. [PubMed: 14718567]

[6]. Duguay D, Foty RA, Steinberg MS. Cadherin-mediated cell adhesion and tissue segregation: qualitative and quantitative determinants. Dev Biol. 2003; 253:309–323. [PubMed: 12645933]

[7]. Dean DM, Morgan JR. Cytoskeletal-mediated tension modulates the directed self-assembly of microtissues. Tissue Eng Part A. 2008; 14:1989–1997. [PubMed: 18673088]

[8]. Califano JP, Reinhart-King CA. A balance of substrate mechanics and matrix chemistry regulates endothelial cell network assembly. Cell Mol Bioeng. 2008; 1:122–132.

[9]. George EL, Georges-Labouesse EN, Patel-King RS, Rayburn H, Hynes RO. Defects in mesoderm, neural tube and vascular development in mouse embryos lacking fibronectin. Development. 1993; 119:1079–1091. [PubMed: 8306876]

[10]. Dzamba BJ, Jakab KR, Marsden M, Schwartz MA, DeSimone DW. Cadherin adhesion, tissue tension, and noncanonical Wnt signaling regulate fibronectin matrix organization. Developmental Cell. 2009; 16:421–432. [PubMed: 19289087]

[11]. Sevilla CA, Dalecki D, Hocking DC. Extracellular matrix fibronectin stimulates the self-assembly of microtissues on native collagen gels. Tissue Eng A. 2010; 16:3805–3819.

[12]. Cseh B, Fernandez-Sauze S, Grall D, Schaub S, Doma E, Van Obberghen-Schilling E. Autocrine fibronectin directs matrix assembly and crosstalk between cell-matrix and cell-cell adhesion in vascular endothelial cells. J Cell Sci. 2010; 123:3989–3999. [PubMed: 20980391]

[13]. Sottile J, Hocking DC. Fibronectin polymerization regulates the composition and stability of extracellular matrix fibrils and cell-matrix adhesions. Mol Biol Cell. 2002; 13:3546–3559. [PubMed: 12388756]

[14]. Hocking DC, Sottile J, Langenbach KJ. Stimulation of integrin-mediated cell contractility by fibronectin polymerization. J Biol Chem. 2000; 275:10673–10682. [PubMed: 10744764]

[15]. Bourdoulous S, Orend G, MacKenna DA, Pasqualini R, Ruoslahti E. Fibronectin matrix regulates activation of RHO and CDC42 GTPases and cell cycle progression. J Cell Biol. 1998; 143:267–276. [PubMed: 9763437]

[16]. da Rocha-Azevedo B, Ho CH, Grinnell F. Fibroblast cluster formation on 3D collagen matrices requires cell contraction-dependent fibronectin matrix organization. Exp Cell Res. 2013; 319:546–555. [PubMed: 23117111]

[17]. Lefort CT, Wojciechowski K, Hocking DC. N-cadherin cell-cell adhesion complexes are regulated by fibronectin matrix assembly. J Biol Chem. 2011; 286:3149–3160. [PubMed: 21084302]

[18]. Hocking DC, Chang CH. Fibronectin matrix polymerization regulates small airway epithelial cell migration. Am J Lung Cell Mol Physiol. 2003; 285:169–179.

[19]. Kenny HA, Chiang CY, White EA, Schryver EM, Habis M, Romero IL, Ladanyi A, Penicka CV, George J, Matlin K, Montag A, Wroblewski K, Yamada SD, Mazar AP, Bowtell D, Lengyel E. Mesothelial cells promote early ovarian cancer metastasis through fibronectin secretion. J Clin Invest. 2014; 124:4614–4628. [PubMed: 25202979]

[20]. Mao Y, Schwarzbauer JE. Fibronectin fibrillogenesis, a cell-mediated matrix assembly process. Matrix Biol. 2005; 24:389–399. [PubMed: 16061370]

[21]. Hocking DC, Kowalski K. A cryptic fragment from fibronectin's III1 module localizes to lipid rafts and stimulates cell growth and contractility. J Cell Biol. 2002; 158:175–184. [PubMed: 12105189]

[22]. Gui L, Wojciechowski K, Gildner CD, Nedelkovska H, Hocking DC. Identification of the heparin-binding determinants within fibronectin repeat III1: role in cell spreading and growth. J Biol Chem. 2006; 281:34816–34825. [PubMed: 16982604]

[23]. Hocking DC, Titus PA, Sumagin R, Sarelius IH. Extracellular matrix fibronectin mechanically couples skeletal muscle contraction with local vasodilation. Circ Res. 2008; 102:372–379. [PubMed: 18032733]

[24]. Zhong C, Chrzanowska-Wodnicka M, Brown J, Belkin AM, Burridge K. Rho-mediated contractility exposes a cryptic site in fibronectin and induces fibronectin matrix assembly. J Cell Biol. 1998; 141:539–551. [PubMed: 9548730]

[25]. Ohashi T, Kiehart DP, Erickson HP. Dynamics and elasticity of the fibronectin matrix in living cell culture visualized by fibronectin-green fluorescent protein. Proc Nat Acad Sci USA. 1999; 96:2153–2158. [PubMed: 10051610]

[26]. Smith ML, Gourdon D, Little WC, Kubow KE, Eguiluz RA, Luna-Morris S, Vogel V. Force-induced unfolding of fibronectin in the extracellular matrix of living cells. PLoS Biol. 2007; 5:e268. [PubMed: 17914904]

[27]. Ambesi A, McKeown-Longo PJ. Conformational remodeling of the fibronectin matrix selectively regulates VEGF signaling. J Cell Sci. 2014; 127:3805–3816. [PubMed: 24982443]

[28]. Gildner CD, Roy DC, Farrar CS, Hocking DC. Opposing effects of collagen I and vitronectin on fibronectin fibril structure and function. Matrix Biol. 2014; 34:33–45. [PubMed: 24509439]

[29]. Sevilla CA, Dalecki D, Hocking DC. Regional fibronectin and collagen fibril co-assembly directs cell proliferation and microtissue morphology. PLoS ONE. 2013; 8:e77316. [PubMed: 24116223]

[30]. Ao M, Brewer BM, Yang L, Franco Coronel OE, Hayward SW, Webb DJ, Li D. Stretching fibroblasts remodels fibronectin and alters cancer cell migration. Sci Rep. 2015; 5:8334. [PubMed: 25660754]

[31]. Wang K, Andresen Eguiluz RC, Wu F, Seo BR, Fischbach C, Gourdon D. Stiffening and unfolding of early deposited-fibronectin increase proangiogenic factor secretion by breast cancer-associated stromal cells. Biomaterials. 2015; 54:63–71. [PubMed: 25907040]

[32]. Li B, Moshfegh C, Lin Z, Albuschies J, Vogel V. Mesenchymal stem cells exploit extracellular matrix as mechanotransducer. Sci Rep. 2013; 3:2425. [PubMed: 23939587]

[33]. Roy DC, Wilke-Mounts SJ, Hocking DC. Chimeric fibronectin matrix mimetic as a functional growth- and migration-promoting adhesive substrate. Biomaterials. 2011; 32:2077–2087. [PubMed: 21185596]

[34]. Tomasini-Johansson BR, Kaufman NR, Ensenberger MG, Ozeri V, Hanski E, Mosher DF. A 49-residue peptide from adhesin F1 of *Streptococcus pyrogenes* inhibits fibronectin matrix assembly. J Biol Chem. 2001; 276:23430–23439. [PubMed: 11323441]

[35]. Copie V, Tomita Y, Akiyama SK, Aota S, Yamada KM, Venable RM, Pastor RW, Krueger S, Torchia DA. Solution structure and dynamics of linked cell attachment modules of mouse fibronectin containing the RGD and synergy regions: comparison with the human fibronectin crystal structure. J Mol Biol. 1998; 277:663–682. [PubMed: 9533887]

[36]. Roy DC, Hocking DC. Recombinant fibronectin matrix mimetics specify integrin adhesion and extracellular matrix assembly. Tissue Eng A. 2013; 19:558–570.

[37]. Roy DC, Mooney NA, Raeman CH, Dalecki D, Hocking DC. Fibronectin matrix mimetics promote full-thickness wound repair in diabetic mice. Tissue Eng A. 2013; 19:2517–2526.

[38]. Akiyama SK. Purification of fibronectin. Curr Prot Cell Biol 10-5. 1999

[39]. Sottile J, Hocking DC, Swiatek PJ. Fibronectin matrix assembly enhances adhesion-dependent cell growth. J Cell Sci. 1998; 111:2933–2943. [PubMed: 9730985]

[40]. McClay, DR.; Hertzler, PL. Vol. 1. John Wiley & Sons, Inc.; 1998. Quantitative measurement of cell adhesion using centrifugal force; p. 9.2.1-9.2.10.Curr Protoc Cell Biol

[41]. Channavajjala LS, Eidsath A, Saxinger WC. A simple method for measurement of cell-substrate attachment forces: application to HIV-1 Tat. J Cell Sci. 1997; 110:249–256. [PubMed: 9044055]

[42]. Reyes CD, Garcia AJ. A centrifugation cell adhesion assay for high-throughput screening of biomaterial surfaces. J Biomed Mater Res A. 2003; 67:328–333. [PubMed: 14517892]

[43]. Gallant ND, Michael KE, Garcia AJ. Cell adhesion strengthening: contributions of adhesive area, integrin binding, and focal adhesion assembly. Mol Biol Cell. 2005; 16:4329–4340. [PubMed: 16000373]

[44]. Ishizaki T, Uehata M, Tamechika I, Keel J, Nonomura K, Maekawa M, Narumiya S. Pharmacological properties of Y-27632, a specific inhibitor of rho-associated kinases. Mol Pharmacol. 2000; 57:976–983. [PubMed: 10779382]

[45]. Obara M, Kang MS, Yamada KM. Site-directed mutagenesis of the cell-binding domain of human fibronectin: separable, synergistic sites mediate adhesive function. Cell. 1988; 53:649–657. [PubMed: 3286012]

[46]. Koivunen E, Wang B, Ruoslahti E. Phage libraries displaying cyclic peptides with different ring sizes: ligand specificities of the RGD-directed integrins. Biotechnology (N Y). 1995; 13:265–270. [PubMed: 9634769]

[47]. Aota S, Nagai T, Yamada KM. Characterization of regions of fibronectin besides the arginine-glycine-aspartic acid sequence required for adhesive function of the cell-binding domain using site-directed mutagenesis. J Biol Chem. 1991; 266:15938–15943. [PubMed: 1874740]

[48]. Wong JY, Weng Z, Moll S, Kim S, Brown CT. Identification and validation of a novel cell-recognition site (KNEED) on the 8th type III domain of fibronectin. Biomaterials. 2002; 23:3865–3870. [PubMed: 12164191]

[49]. Wan AM, Chandler EM, Madhavan M, Infanger DW, Ober CK, Gourdon D, Malliaras GG, Fischbach C. Fibronectin conformation regulates the proangiogenic capability of tumor-associated adipogenic stromal cells. Biochim Biophys Acta. 2013; 1830:4314–4320. [PubMed: 23567798]

[50]. Grant RP, Spitzfaden C, Altroff H, Campbell ID, Mardon HJ. Structural requirements for biological activity of the ninth and tenth FIII domains of human fibronectin. J Biol Chem. 1997; 272:6159–6166. [PubMed: 9045628]

[51]. Krammer A, Craig D, Thomas WE, Schulten K, Vogel V. A structural model for force regulated integrin binding to fibronectin's RGD-synergy site. Matrix Biol. 2002; 21:139–147. [PubMed: 11852230]

[52]. Lotz MM, Burdsal CA, Erickson HP, McClay DR. Cell adhesion to fibronectin and tenascin: quantitative measurements of initial binding and subsequent strengthening response. J Cell Biol. 1989; 109:1795–1805. [PubMed: 2477381]

[53]. Sottile J, Shi F, Rublyevska I, Chiang HY, Lust J, Chandler J. Fibronectin-dependent collagen I deposition modulates the cell response to fibronectin. Am J Physiol Cell Physiol. 2007; 293:C1934–1946. [PubMed: 17928541]

[54]. Ryan PL, Foty RA, Kohn J, Steinberg MS. Tissue spreading on implantable substrates is a competitive outcome of cell-cell vs. cell-substratum adhesivity. Proc Nat Acad Sci USA. 2001; 98:4323–4327. [PubMed: 11274361]

[55]. Guven S, Chen P, Inci F, Tasoglu S, Erkmen B, Demirci U. Multiscale assembly for tissue engineering and regenerative medicine. Trends Biotechnol. 2015; 33:269–279. [PubMed: 25796488]

[56]. McKeown-Longo PJ, Etzler CA. Induction of fibronectin matrix assembly in human fibrosarcoma cells by dexamethasone. J Cell Biol. 1987; 104:601–610. [PubMed: 2950120]

[57]. Schwarz MA, Zheng H, Legan S, Foty RA. Lung self-assembly is modulated by tissue surface tensions. Am J Respir Cell Mol Biol. 2010; 44:682–691. [PubMed: 20616358]

[58]. Singh P, Schwarzbauer JE. Fibronectin matrix assembly is essential for cell condensation during chondrogenesis. J Cell Sci. 2014; 127:4420–4428. [PubMed: 25146392]

[59]. Sabari J, Lax D, Connors D, Brotman I, Mindrebo E, Butler C, Entersz I, Jia D, Foty RA. Fibronectin matrix assembly suppresses dispersal of glioblastoma cells. PLoS One. 2011; 6:e24810. [PubMed: 21980357]

[60]. Sottile J, Chandler J. Fibronectin matrix turnover occurs through a caveolin-1-dependent process. Mol Biol Cell. 2005; 16:757–768. [PubMed: 15563605]

[61]. Parsons JT, Horwitz AR, Schwartz MA. Cell adhesion: integrating cytoskeletal dynamics and cellular tension. Nat Rev Mol Cell Biol. 2010; 11:633–643. [PubMed: 20729930]

[62]. Winters BS, Raj BK, Robinson EE, Foty RA, Corbett SA. Three-dimensional culture regulates Raf-1 expression to modulate fibronectin matrix assembly. Mol Biol Cell. 2006; 17:3386–3396. [PubMed: 16707572]

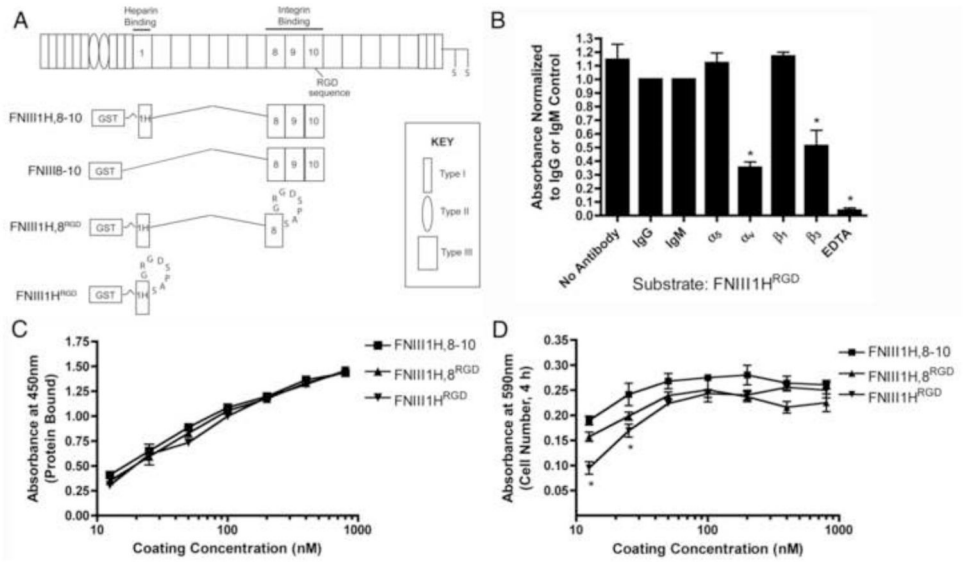

Fig. 1.

Fibronectin matrix mimetics. (A) Schematic representation of a fibronectin subunit and fibronectin fusion proteins. (B) FN-null MEFs were seeded (1.6×10^5 cells/cm^2) onto wells pre-coated with FNIII1H^{RGD} (100 nM) in the presence of integrin function-blocking antibodies, isotype-matched control antibodies, or EDTA. Cell adhesion was determined as described in “Methods”. Data are presented as mean fold difference compared to IgG (α_5, α_v, β_3) or IgM (β_1) controls ± SEM of 3 experiments performed in triplicate. *Significantly different from +IgG, $p < 0.05$ (ANOVA). (C) Tissue culture plates were coated with increasing concentrations of proteins. The relative amount of protein bound to wells was determined by ELISA. Data are presented as mean absorbance of triplicate wells ± SEM and represent of 1 of 4 experiments performed. (D) FN-null MEFs were seeded (1.6×10^5 cells/cm^2) onto protein-coated wells and allowed to attach for 4 h. The number of adherent cells was determined as described in “Methods”. Data are presented as mean absorbance of triplicate wells ± SEM and represent of 1 of 3 experiments performed. *Significantly different from FNIII1H,8^{RGD} and FNIII1H,8-10, $p < 0.05$ (ANOVA).

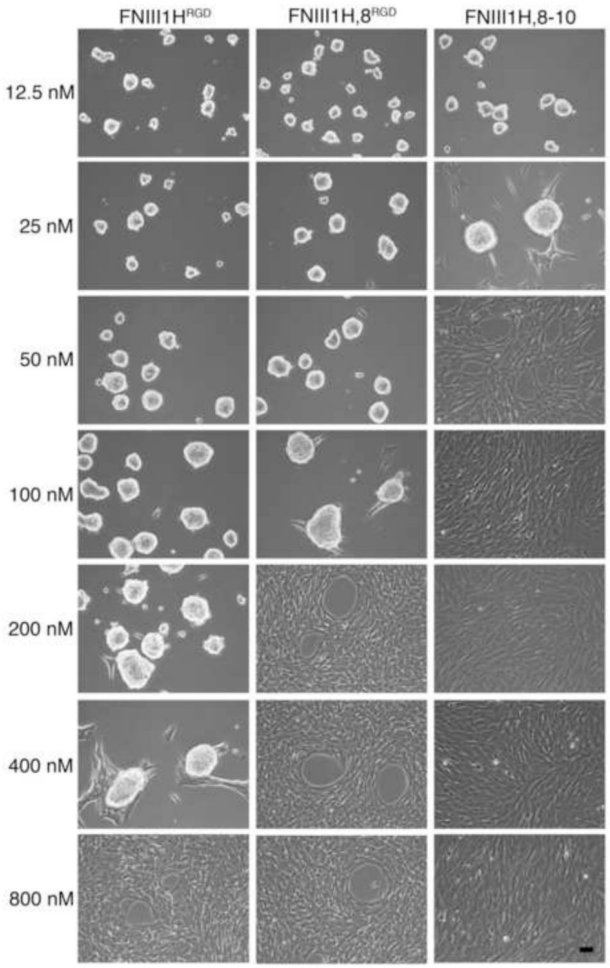

Fig. 2.

Fibronectin matrix mimetics support cellular self-assembly. FN-null MEFs were seeded (2×10^4 cell/cm^2) on tissue culture plates pre-coated with FNIII1H^{RGD}, FNIII1H,8^{RGD}, or FNIII1H,8-10 at coating concentrations ranging from 12.5 – 800 nM. Soluble plasma fibronectin (25 nM) was added 4 h post-seeding. Phase contrast microscopy images were taken at 72 h post-seeding. Images represent 1 of 3 experiments performed. Scale bar, 50 μm.

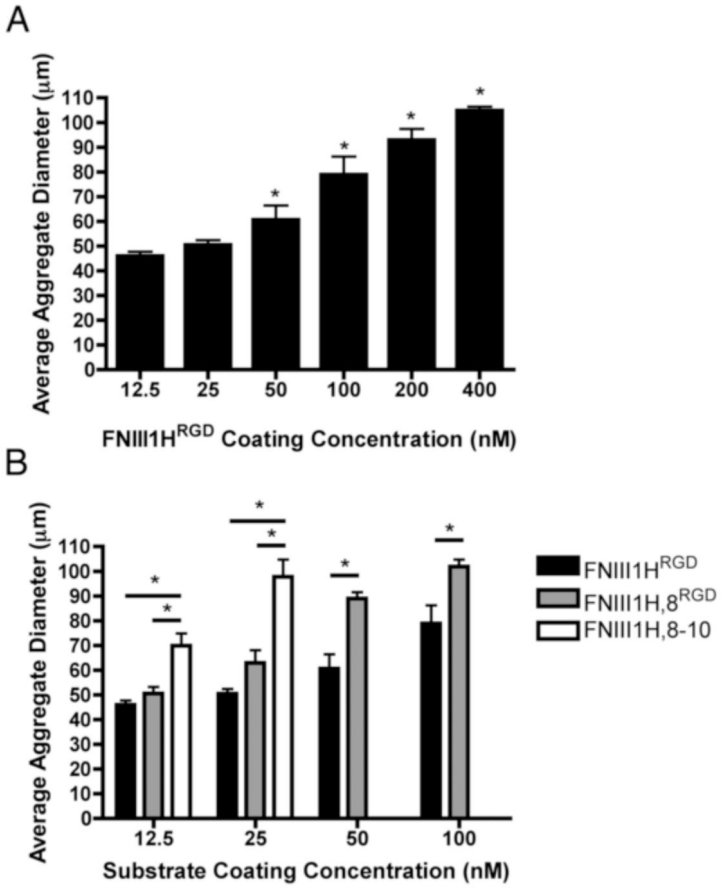

Fig. 3.

Effect of substrate density on aggregate diameter. FN-null MEFs were seeded (2×10^4 cell/cm^2) on wells pre-coated with indicated coating concentrations of FNIII1H^{RGD} (A, B; black bars), FNIII1H,8^{RGD} (B; grey bars) or FNIII1H,8-10 (B; white bars). Soluble plasma fibronectin (25 nM) was added 4 h post-seeding. Phase contrast microscopy images were obtained 72 h post-seeding, capturing at least 30 aggregates per sample. Spheroid diameter was quantified from images using ImageJ. Data are presented as mean aggregate diameter ± SEM of 3 experiments. (A) *Significantly different from 12.5 nM, $p < 0.05$; (B) *Significantly different, $p < 0.05$ (ANOVA).

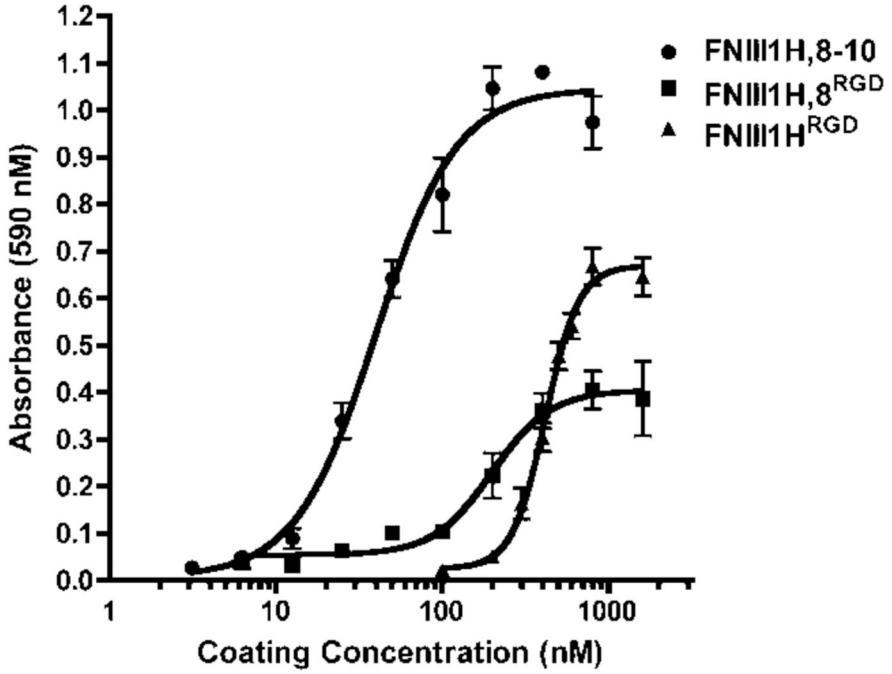

Fig. 4.

Initial cell-substrate binding strength of fibronectin matrix mimetics. Tissue culture plates (96-well) were pre-coated with increasing concentrations of FNIII1H^{RGD}, FNIII1H,8^{RGD}, or FNIII1H,8-10. FN-null MEFs (1.6×10^5 cell/cm^2) were added to wells on ice and centrifugal adhesion assays were performed as described in “Methods”. GraphPad Prism was used to fit a sigmoidal curve to the data. Data are presented as mean absorbance of triplicate wells ± SEM and represent 1 of at least 3 independent experiments performed.

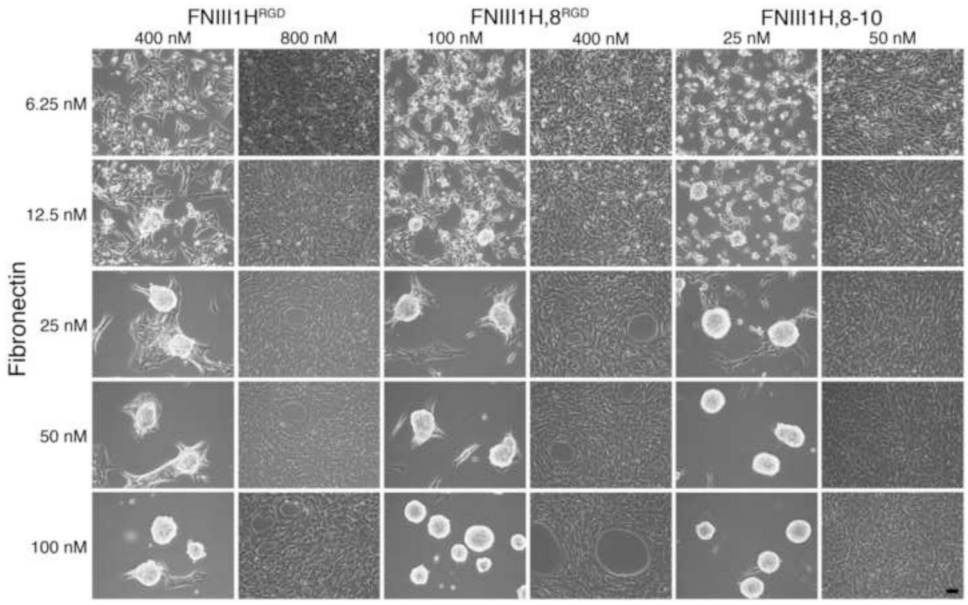

Fig. 5.

Bimodal response to soluble fibronectin. FN-null MEFs were seeded (2×10^4 cells/cm^2) on tissue culture plates pre-coated with fibronectin matrix mimetics at concentrations above and below the initial C^{c50} value (400 nM and 800 nM for FNIII1H^{RGD}; 100 nM and 400 nM for FNIII1H,8^{RGD}; 25 nM and 50 nM for FNIII1H,8-10). Four h after seeding, cells were treated with various concentrations of soluble fibronectin (6.25 – 100 nM). Microscopy images were taken at 72 h post-seeding. Images represent 1 of 3 experiments performed. Scale bar, 50 μm.

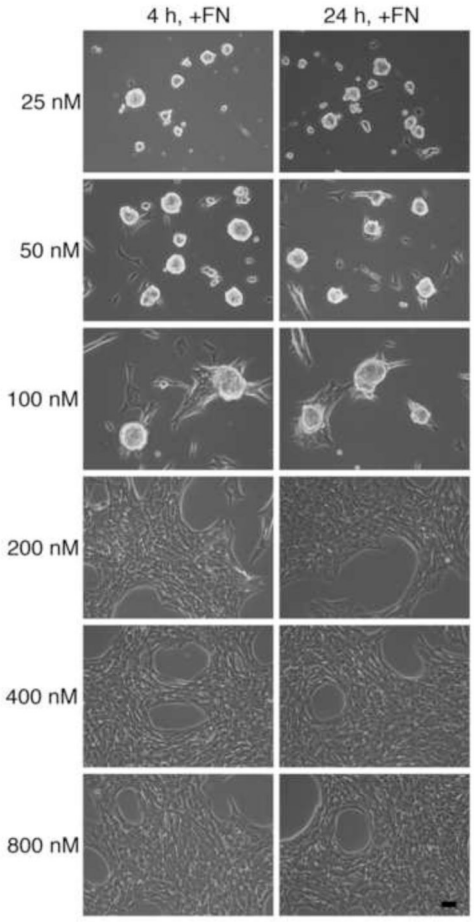

Fig. 6.

Fibronectin-induced cellular self-assembly at early and late stages of cell spreading. FN-null MEFs were seeded (2×10^4 cells/cm^2) on tissue culture plates pre-coated with FNIII1H, 8^{RGD} at various concentrations (25 - 800 nM). At either 4 h or 24 h after seeding, cells were treated with soluble fibronectin (25 nM). Phase contrast microscopy images were taken at 72 h post-seeding. Images represent 1 of 3 experiments performed. Scale bar, 50 μm.

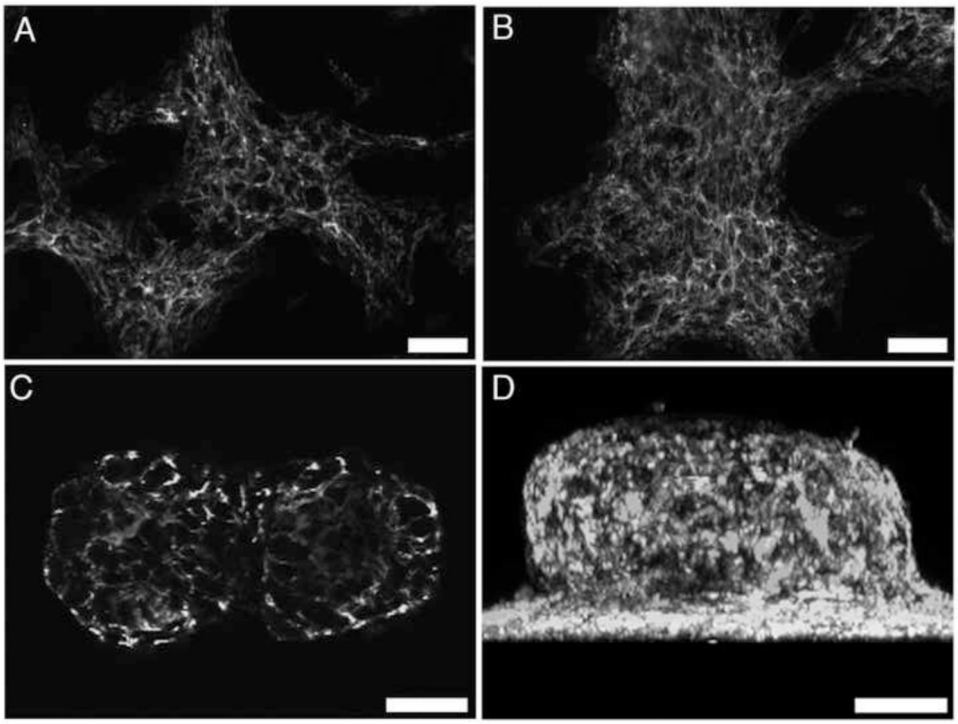

Fig. 7.

Fibronectin fibril formation within 3D aggregates. FN-null MEFs were seeded (2×10^4 cells/cm^2) onto plates pre-coated with 400 nM FNIII1H^{RGD}, allowed to adhere for 4 h, and then treated with 25 nM fibronectin. Cells were processed for immunofluorescence microscopy at 24 (A), 48 (B), or 72 (C,D) h post-seeding and immunostained for fibronectin. Images were collected along the z-axis at 1μm intervals using two-photon microscopy. Image in (C) is a representative slice taken 40 μm above the surface of the culture plate. (D) Z-slice images were reconstructed in 3D and projected along the x-y plane. Images represent 1 of 3 experiments performed. Scale bars, 50 μm.

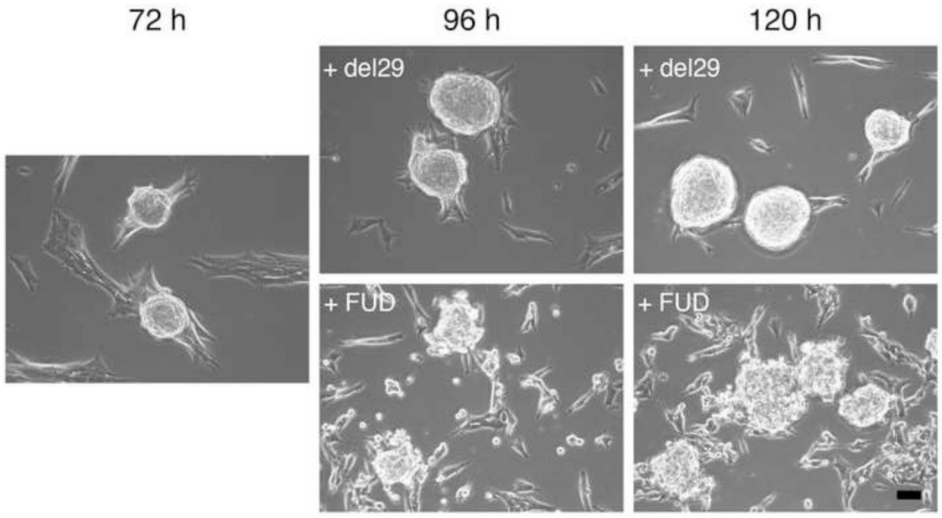

Fig. 8.

Fibronectin matrix assembly maintains aggregate cohesion. FN-null MEFs were seeded (2×10^4 cells/cm^2) onto plates pre-coated with 400 nM FNIII1H^{RGD}. At 4 h post-seeding, 25 nM fibronectin was added to initiate aggregate formation. At 72 h post-seeding, phase contrast microscopy images were obtained, and FUD peptides (250 nM) were added directly to wells to inhibit fibronectin matrix assembly. Control wells received the inactive control, del29 (250 nM). Samples were incubated for an additional 2 d and images were obtained on each day, at 96 h and 120 h post-seeding. Images represent 1 of 3 experiments performed. Scale bars, 50 μm.

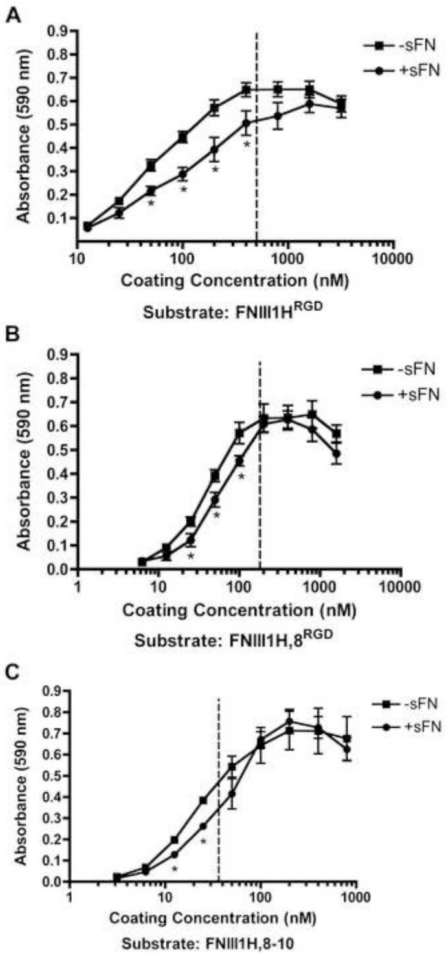

Fig. 9.

Fibronectin decreases cell-substrate attachment strength during cellular self-assembly. FN-null MEFs were seeded (4×10^4 cells/cm^2) onto tissue culture plates pre-coated with increasing concentrations of FNIII1H^{RGD}, FNIII1H,8^{RGD}, or FNIII1H,8-10 and allowed to adhere for 4 h. Cells were then incubated in the absence (−sFN) or presence (+sFN) of soluble fibronectin (50 nM) for an additional 20 h. Centrifugal cell adhesion assays were performed and the number of cells that remained adherent was determined, as described in "Methods". Data are presented as mean absorbance ± SEM of at least 3 separate experiments, each performed in triplicate. *Significantly different from corresponding '−sFN', $p < 0.05$ (t-test). The dotted lines denote the initial Cc^{50} values.

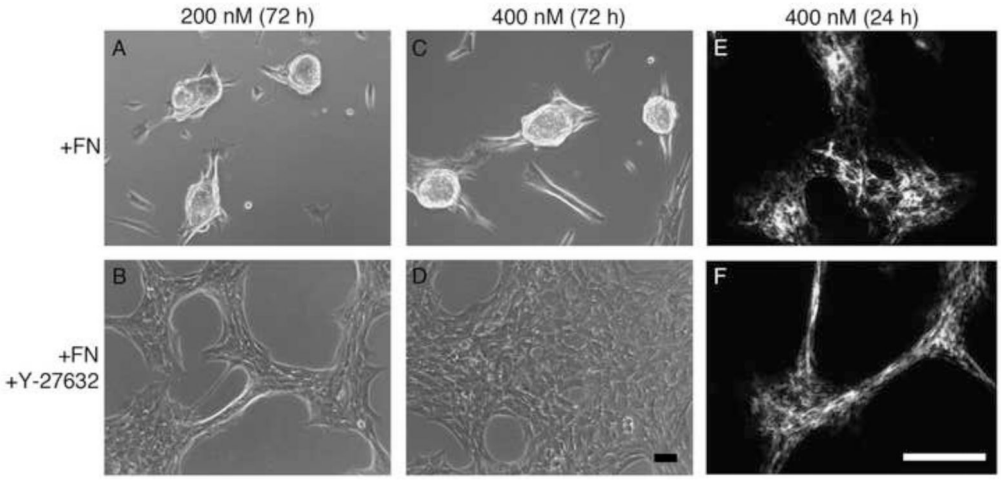

Fig. 10.

Effect of Rho inhibition on fibronectin-mediated cellular self-assembly. FN-null MEFs were seeded (2×10^4 cells/cm^2) onto tissue culture plates pre-coated with 200 nM (A, B) or 400 nM (C-F) FNIII1H^{RGD}, in the presence of either 10 μM Y-27632 (B, D, F) or an equal volume of the vehicle, PBS (A, C, E). At 4 h post-seeding, cells were treated with 25 nM soluble fibronectin (+sFN) and incubated for up to 3 d. At 72 h post-seeding, phase contrast microscopy images were obtained (A-D). At 24 h post-seeding, some wells were processed for immunofluorescence microscopy and fibronectin fibrils were visualized using polyclonal anti-fibronectin antibodies (E, F). Images represent 1 of 3 experiments performed. Scale bars, 50 μm.

Table 1

Cell-substrate binding strengths for fibronectin matrix mimetics. Values representing the inverse adhesive affinity for full-length fibronectin and various fibronectin fragments were determined by determining the coating concentration required for half-maximal adhesion (C_C^{50}; nM) in centrifugal adhesion assays. Initial adhesion strength (C_C^{50}, initial) was determined by centrifuging cells into contact with substrates for 3 min at 4°C. Adhesion strength was also determined at 24 h post-seeding for cells cultured in the absence (−sFN) and presence (+sFN) of soluble fibronectin (50 nM). Data are presented as mean coating concentration (nM) ± SEM and were determined from at least 3 independent experiments performed in triplicate.

Substrate	**C_c^{50}, Initial**	**C_c^{50}, 24 h, −sFN**	**C_c^{50}, 24 h, +sFN**
FNIII1H^{RGD}	499 ± 44.2*	43.8 ± 2.00	82.5 ± 10.6+
FNIII1H,8^{RGD}	177 ± 11.1*	40.6 ± 2.72	55.5 ± 5.00+
FNIII1H,8-10	36.1 ± 5.90	35.0 ± 4.04	46.1 ± 7.76
FNIII8-10	24.4 ± 3.54	n.d.	n.d.
Fibronectin	22.6 ± 2.38	n.d.	n.d.

n.d., not done.

*Initial C_C^{50} values are significantly different from ‘Fibronectin’, $p<0.5$ (ANOVA);

+Significantly different from corresponding C_C^{50}, 24 h, −sFN, $p<0.05$ (unpaired *t*-test);